A uniaxial bioMEMS device for imaging single cell response during quantitative force-displacement measurements

**David B. Serrell · Jera Law · Andrew J. Slifka ·
Roop L. Mahajan · Dudley S. Finch**

Abstract A microfabricated device has been developed for imaging of a single, adherent cell while quantifying force under an applied displacement. The device works in a fashion similar to that of a displacement-controlled uniaxial tensile machine. The device was calibrated using a tipless atomic force microscope (AFM) cantilever and shows excellent agreement with the calculated spring constant. A step input was applied to a single, adherent fibroblast cell and the viscoelastic response was characterized with a mechanical model. The adherent fibroblast was imaged by use of epifluorescence and phase contrast techniques.

Keywords Actin · BioMEMS · Fibroblasts ·
Micro-fabricated · Single-cell

1 Introduction

We have developed a MEMS-based, single-cell measurement technique that allows mechanical force-displacement data to be taken while simultaneously imaging the living cell. Mechanical forces have profound effects on cellular function and behavior. Cells are nonlinear, viscoelastic, and constantly adaptive; they rapidly sense changes in their mechanical environment and adapt their internal structure and function in response. Mechanical stresses on cells can influence cellular processes such as growth, differentiation, apoptosis, contraction, division, spreading and the regulation of protein transduction (Chicurel et al. 1998; Maniotis et al. 1997; Janmey 1998; Lenormand and Fredburg 2006; Janmey and McCulloch 2007). Furthermore, several well known pathologies such as sickle cell anemia and asthma are related to the mechanical properties of cells. Despite the importance of forces on cell life, the underlying mechanisms for how these forces are transmitted and regulated within living cells are poorly understood. To quantify the relationship between mechanical force and cellular response, there is a need for accurate, physical metrology tools that can determine time-dependent, force-displacement responses in living cells and simultaneously integrate this data with imaging of subcellular structures.

There are a wide variety of techniques available to quantify mechanical forces on single cells in vitro. Techniques such as atomic force microscopy (Hyonchol et al. 2002; Yamamoto et al. 1998; Mathur et al. 2001; Florin et al. 1994), magnetic traps (Wang et al. 1993; Chen et al. 2001; Lo et al. 1998; Alenghat et al. 2000; Lenormand and Fredburg 2006; Deng et al. 2006), optical traps (Svoboda and Block 1994; Yamada et al. 2000) and silicon cantilevers (Saif et al. 2003; Saif et al. 2002) have been used for studying local cellular phenomena as well as individual components of the cystoskeleton such as actin (Minajeva et al. 2001; Zaner and Valberg 1989). Other techniques used to study single-cell mechanics at the global level include micropipette aspiration (Evans and Yeung 1989; Evans and Hochmuth 1976; Hochmuth 1981; Hochmuth and Waugh 1987), flexible silicon substrates (Di Palma et al. 2003; Ignatius et al. 2004; Moretti et al. 2004; Park et al. 2004), shear flow devices (Ainslie et al. 2005; Rhodes et al. 1998;

D. B. Serrell (✉) · J. Law · A. J. Slifka
National Institute of Standards and Technology,
Boulder, CO, USA
e-mail: david.serrell@colorado.edu

D. B. Serrell
University of Colorado,
Boulder, CO, USA

R. L. Mahajan · D. S. Finch
Virginia Polytechnic Institute and State University,
Blacksburg, VA, USA

Soghomonians et al. 2005), glass microplates (Desprat et al. 2005; Thoumine and Ott 1997) and silicon cantilevers (Yang and Saif 2005). A MEMS device that has been designed for biaxial stimulation of cells but has not been demonstrated on a living cell has been described (Scuor et al. 2006). Recent reviews of these mechanical methods can be found in the literature (Addae-Mensah and Wikswo 2008; Desai et al. 2007). While each technique has strengths and limitations, none is specifically designed to correlate mechanical data with cytoskeletal morphology.

This paper describes a novel, microfabricated device designed to measure the mechanical properties of an entire, adherent single cell while simultaneously allowing imaging of the cell. The device utilizes microactuators and microsensors to quantify and manipulate a single cell. The operation of the device is described as well as the actuation and sensing techniques used. The sensor was calibrated using an atomic force microscope (AFM) cantilever. To demonstrate the device, a single fibroblast was placed on the cell platform, imaged, and its force response to an applied displacement was measured. Cell culturing and placement techniques are also described.

2 Methods

2.1 Cell puller

A single cell was placed on a transparent, platform [CP in Fig. 1(a)] that is circular and divided in two parts. The cell was allowed to adhere, after which a displacement was applied to one half of the cell platform [through PA, in Fig. 1(a)] while the other half was mechanically linked to a sensor that can measure the force on the cell. The actuation was provided by an off-chip, computer controlled piezo-electric stage while the sensor was several cantilever beams in parallel. This device was based on a previously developed prototype that lacked the imaging capabilities of the current device (Serrell et al. 2007).

2.2 Device fabrication

The devices were fabricated by use of a custom process that consists of a single structural, single-crystal silicon (SCS) layer combined with a silicon nitride structural layer over a silicon oxide sacrificial layer. The cell platform consists of an
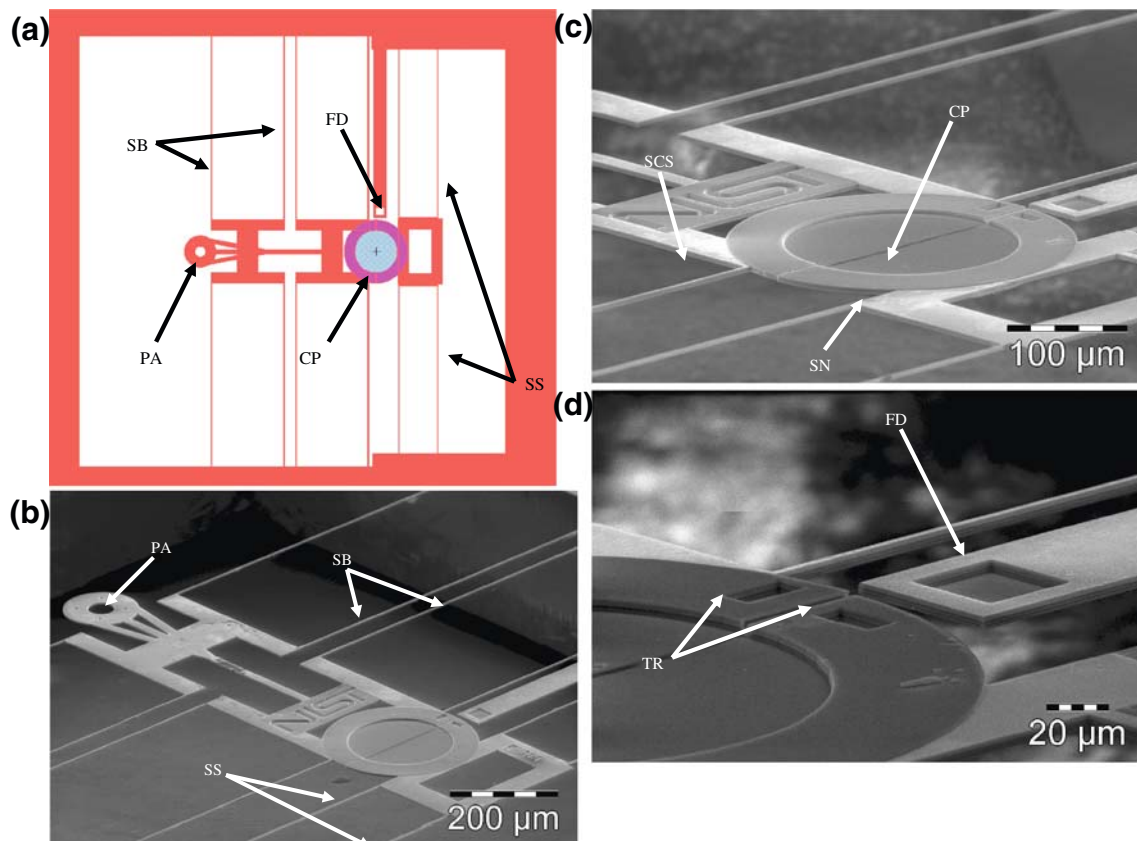

Fig. 1 A schematic drawing of the transparent cell puller (**a**): the central cell platform (*CP*), the support beams (*SB*) for the annulus (*PA*) and the sensor springs (*SS*). The SEM photo (**b**) shows the finished device. The single crystal silicon (*SCS*) and the optically transparent silicon nitride (*SN*) make up the cell platform (**c**). The platform displacement is tracked using a stationary fiducial mark (*FD*), tracking marks (*TR*) and image tracking software (**d**)

800 nm silicon nitride membrane suspended by a SCS annulus. This provides the transparent substrate onto which the cell can adhere. A backside etch through the wafer allows an optical path through the entire cell platform. When released, the adherent cell on the silicon nitride platform can be imaged.

Devices are fabricated using commercially available silicon-on-insulator (SOI) wafers (Fig. 2). The wafers consist of a single-crystal silicon handle wafer of thickness 400 μm with a layer of silicon oxide (10 μm) and another single-crystal silicon device layer (5 μm) bonded on top. The device is formed by etching through the silicon device layer, depositing the transparent thin film and then etching away the oxide layer, leaving free-standing structures.

The relatively high aspect ratios between the device layer and the oxide substrate can cause problems when etching, in the form of uneven photoresist distribution. This can leave certain structures poorly covered with resist and result in uneven etching of the subsequent layer. To minimize this problem, the etching of the device was carried out in two steps. The cell platform via was etched first by use of a deep reactive ion etching (DRIE), which allowed for rapid etching and near vertical sidewalls. The first etch defined the area where the transparent membrane will be formed. Silicon nitride was then deposited by use of a low pressure chemical vapor deposition (LPCVD) to a depth of 800 nm. Thickness was verified using an ellipsometer. The silicon nitride was patterned and etched by use of a reactive ion etcher (RIE). The wafer was then patterned and the remaining structures that define the pulling annulus, sensor springs, and all support beams are etched by the DRIE. The back of the wafer was patterned and the silicon nitride on the backside was etched in the RIE. The wafer was then bonded to another handle wafer to protect the surface features during the backside etch. The backside etch was carried out in the DRIE system with the oxide layer as an etch stop. The backside etch allows for a light path through the transparent cell platform and it also was used to dice individual chips from the bulk wafer.

The release process was carried out in a fashion similar to earlier designs with modifications for the transparent substrate and backside etch (Serrell et al. 2007). The chips were glued to a 25 mm Petri dish and then wet-etched with hydrofluoric acid. At the completion of the etch, the acid was drained and replaced with deionized (DI) water. Because of the backside etch, bubbles became trapped beneath the suspended cell puller device and the Petri dish. A 30 min soak with methanol allowed the bubbles to slip past the cell puller devices without damaging them. The chip was then allowed to soak in DI water for 12 h. The released chip was never exposed directly to air and never allowed to dry. By utilizing this release process, delicate structures can be fabricated that would not normally survive the transition from air to water.
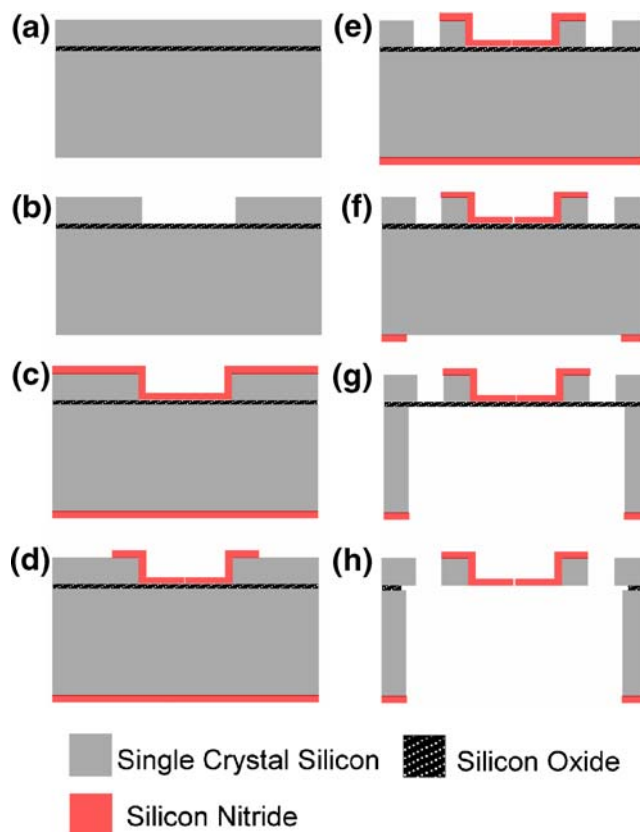

Fig. 2 The process for fabricating the transparent pullers utilizes silicon-on-insulator (SOI) wafers (a). The DRIE was utilized for etching of the single crystal silicon (SCS) in two steps. The first etch defined the cell platform (b). The nitride was then deposited and etched with an RIE (c, d). The remaining SCS structures were etched (e) with the DRIE. The backside etch was completed with the DRIE (g) and the devices are released in HF (h)

Devices that were imaged with the scanning electron microscope (SEM) were released vertically in hydrofluoric acid, rinsed in DI water, rinsed in methanol and allowed to air dry at room temperature.

After release, the chip was prepared for the experiment by draining the DI water and rinsing with phosphate-buffered saline (PBS). The Petri dish containing the chip was then filled with a solution of 20 μl of 0.1% fibronectin and 780 μl of PBS, for a concentration of 25 μM, and placed in an incubator for 4 h.

The displacement was applied to the cell platform by use of a standard probe tip driven by a commercially available, off-chip piezoelectric stage with a resolution of 0.4 nm. A silicon annulus was attached to the cell platform by a silicon beam supported by several cantilever springs. The probe tip was inserted into an annulus at the end opposite the cell platform. The actuation method has the ability to produce large displacements limited only by spring geometry and piezoelectric stage parameters. The maximum displacement of the actuator is approximately 50 μm, at which point the platform buckles laterally. By changing the

geometry of the springs used to guide and support the cell platform, the displacement limits and frequency of cyclic loads can be varied, limited only by the speed of the piezoelectric. Here, it was limited to approximately 520 Hz. Because the piezoelectric stage is not submerged in cell media, no electrical connection to the actual device was required simplifying the packaging.

The sensing side of the device was based on several cantilever beams arrayed in parallel to create a spring. By designing the springs with a known spring constant and measuring displacement of the sensor side of the cell platform, the force on the cell can be measured.

The theoretical spring constant was calculated to allow springs to be designed in the appropriate force range for single cell studies. The spring constant of the folded-beam springs can be calculated from standard beam theory. The springs consist of four, fixed-fixed cantilever beams in parallel. Each beam was composed of two cantilever beams in series. From simple beam theory, the sensors spring constant is:

$$k_{L/2} = \frac{3EI}{(L/2)^3} = \frac{2Ehw^3}{L^3} \qquad (1)$$

$$k_{spring} = 4\left(\frac{k_{L/2}}{2}\right) = \frac{4Ew^3h}{L^3} \qquad (2)$$

where E is Young's modulus, I is moment of inertia (Lardner and Archer 1994), L is the beam length, h is the depth of the beam and w is the width. Beams with a width of $w=3$ μm, a device layer of $h=5$ μm and a length L=800 μm can yield a theoretical spring constant of 178.24 nN μm^{-1}. These parameters have proven to be robust enough to survive the fabrication and release process and still be a useful force range for studies of single cells. These parameters can be optimized and tailored to suit a specific cell type or protocol.

The displacement of the cell platform was measured by capturing images at two frames per second with a 3.3 megapixel camera. Images were captured at a rate of two frames per second. A pattern-matching algorithm was used to track the etch holes in the platform and a fiducial mark that remained stationary. By calibrating the images, the motion of the cell platform could be determined within a resolution 50 nm.

2.3 Sensor calibration

The in-plane stiffness of the sensor springs is given by Eq 2. The primary uncertainty in the calculation of k is the geometry of the beams. The thickness of the beams was dictated by the device layer from the SOI wafers, while the beam width was defined by the photolithographic process and the etching of the silicon. The springs were calibrated by use of a commercially available silicon AFM cantilever. The AFM cantilever was a "tip less" design and had been previously calibrated by the manufacturer (Tortonese and Maruyama 1997).

The AFM cantilever was mounted on a custom-made fixture that allowed it to be placed with a micromanipulator in proximity to the springs on the chip. The free end of the AFM cantilever was put in contact with one side of the spring [Fig. 3(a)] at the working angle recommended by the manufacturer (12.5° from vertical). The piezoelectric stage described earlier was then used to move the chip in one micron increments and images were taken of each successive movement. By using this technique, the displacement of the spring and the displacement of the chip relative to the AFM cantilever can both be seen in each frame. The sensor spring constant (k_{spring}) is given by:

$$k_{spring} = \frac{(d - d_1) * k_{AFM}}{d_1}, \qquad (3)$$

where k_{AFM} is the spring constant of the AFM cantilever and d is the displacement of the chip relative to the stationary AFM tip. The primary uncertainty in the calibration occurred when the AFM made contact with the spring. There was usually a small gap between the AFM tip and the spring. Thus, the tip can move some distance before contacting the spring. This gap creates artificially high spring constants at the onset of the experiment. However, the values quickly converge to a range near that of the theoretical value [Fig. 3(b)]. The calibrated spring constant for the average of four runs was found to be 213.06±27.14 nN/μm. The actual dimensions of the spring were measured optically, and the thickness of the silicon was measured using a profilometer. The theoretical spring constant was calculated as 178.24 nN/μm by use of the measured dimensions. The accuracy of the calibration verifies the beam geometry.

2.4 Sample preparation

The cell placement took place on a standard probe station. The Petri dish containing the chip was housed in a commercially available microincubator that maintained the cell media at 37°C throughout the placement process. The commercially available fibroblast cell line (BHK-21) was cultured in T25 cell culture flasks and maintained in DMEM supplemented with 10% fetal bovine serum and 1% antibiotic-antimycotic. The cells were removed from culture with 0.05% trypsin–EDTA before 70% confluence for better individual cell separation. The fibroblasts were centrifuged into pellet form and resuspended in fibroblast media for the experiments. From this suspension, a single

cell was then aspirated into a micropipette tip. The Petri dish containing the chip was rinsed and filled with media. The Petri dish/chip assembly was then placed into the microincubator and the cell was aspirated onto the fibronectin-coated (25 μM) cell platform where it was allowed to adhere. Once the cell had initially adhered (typically, 10 min) it was moved to a full size incubator where it was allowed to adhere for 2 h (Fig. 4).

After the cell had adhered, the chip was moved to an inverted microscope equipped with the data-collection camera and piezoelectric stage where testing took place.

A live/dead viability/cytotoxicity fluorescence microscopy assay was used to visualize the live cell while it was fully

adhered to the platform. Five hundred microliters of the live/dead stain (2 μM calcein AM and 4 μl EthD-1 in PBS) were added to the Petri dish and the cell was incubated at room temperature for 30 min. Another 100 μl of live/dead stain was added prior to visualizing the cell.

3 Results and discussion

A single fibroblast was placed on the cell platform and allowed to adhere for 2 h. An 11 μm step input was applied to the displacement side of the platform [Fig. 5(a)]. The force response of the cell was then measured for approximately 3 min.

The force on the cell was plotted versus time [Fig. 5(b)]. Force was calculated using:

$$F_{cell} = k_{spring} \times d_{sensor}, \tag{4}$$

where k_{spring} is the calibrated spring constant for the spring assembly and d_{sensor} is the displacement of the sensor half of the cell platform. Thus, the cell was strained between the two halves of the cell platform. The viscoelastic response of the cell was modeled by use of the standard linear model:

$$F(t) = u_0 \times \left(k_1 + k_2 \times e^{(-t/\tau)} \right) \tag{5}$$

where u_0 is the initial gap between the two plates of the cell platform immediately following the step input ($t=0$), k_1 and k_2 are elastic constants, t is time, and τ is relaxation time.

The viscoelastic response is typical of single cell response. Various mechanical approaches have been used to model the behavior (Bausch et al. 1999; Ragsdale et al. 1997; Thoumine and Ott 1997) and, more recently, a weak power law has also been used (Fabry et al. 2001; Fabry et al. 2003). The least squares fit of the data to Eq. 5 here yields $k_1=114.15$ nN/μm, $k_2=90.43$ nN/μm and $\tau=52.97$ s.
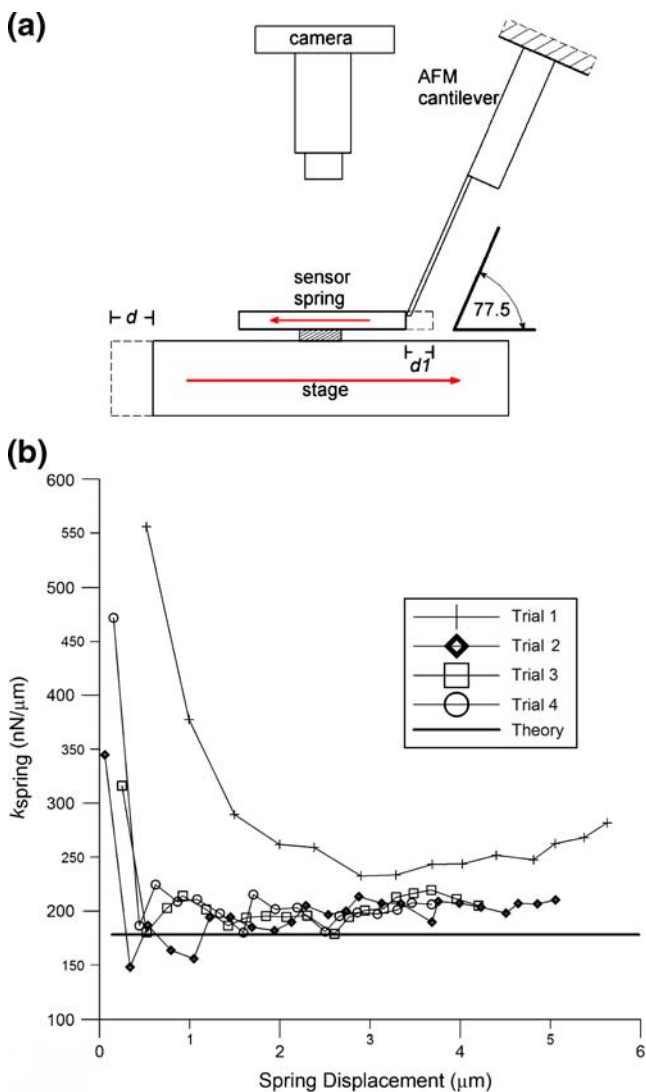

Fig. 3 The calibration setup using a tipless AFM cantilever (**a**). The stage is moved relative to the stationary AFM tip a distance d, resulting in displacement d_1 of the sensor spring. The stage is moved in one micron increments and images of each step are captured. The displacements are then calculated from the images. Calibration curves converge on the theoretical value (**b**)
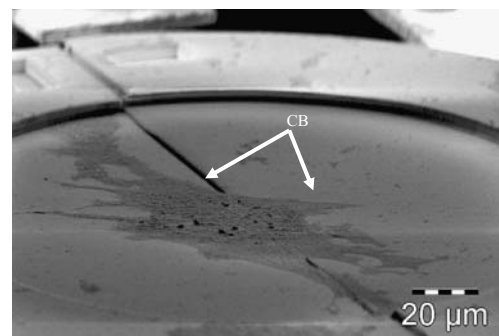

Fig. 4 A single cell (*CB*) is placed in the center of the cell platform for testing. This SEM photo shows a cell that has been placed, allowed to spread and then dried and preserved. The alignment of the cell along the platform gap has a negligible effect on the results

Two other cells were measured using this device, which resulted in values of $k_1=173.24$ nN/μm, $k_2=95.90$ nN/μm, $\tau=38.37$ s and $k_1=192.00$ nN/μm, $k_2=149.71$ nN/μm, $\tau=49.00$ s The data here are presented as a demonstration of the device capabilities.

The relative standard uncertainty of the force measurement comes from several sources. The first is the measurement of the displacement. As stated earlier, the estimated resolution of the displacement is 50 nm. We arrived at this value by tracking a stationary feature over the course of the experiment. The algorithm perceived the stationary object to move a maximum of 50 nm from frame to frame. The second source of uncertainty comes from the AFM cantilever. Tortonese and Maruyama (1997) stated the

error in the calibration of the cantilever tip to be 3.3% and the calibration of the spring was in error with the theory by almost 20%. Thus, the calibration of the springs has the same error Tortonese and Maruyama report. The mounting of the AFM cantilever at 12.5° can be off by several degrees. However, this is considered negligible. Based on the above, we estimate the relative standard uncertainty to be approximately 20% for absolute measurements.

The imaging of the cell was demonstrated by using a live/dead fluorescent dye [Fig. 6(a)]. The green fluorescence shows the cell is viable on the cell platform and also demonstrates the imaging capabilities of the transparent substrate. The cell can be imaged by use of phase contrast [Fig. 6(b)], differential interference contrast, or epifluorescence. By using epifluorescence, for instance, key subcellular components, such as actin, can be labeled and observed after or even in real time during experimentation. Other possibilities include tagging the membrane with particles and tracking the resultant strain field or observing changes in membrane potential with applied strain.
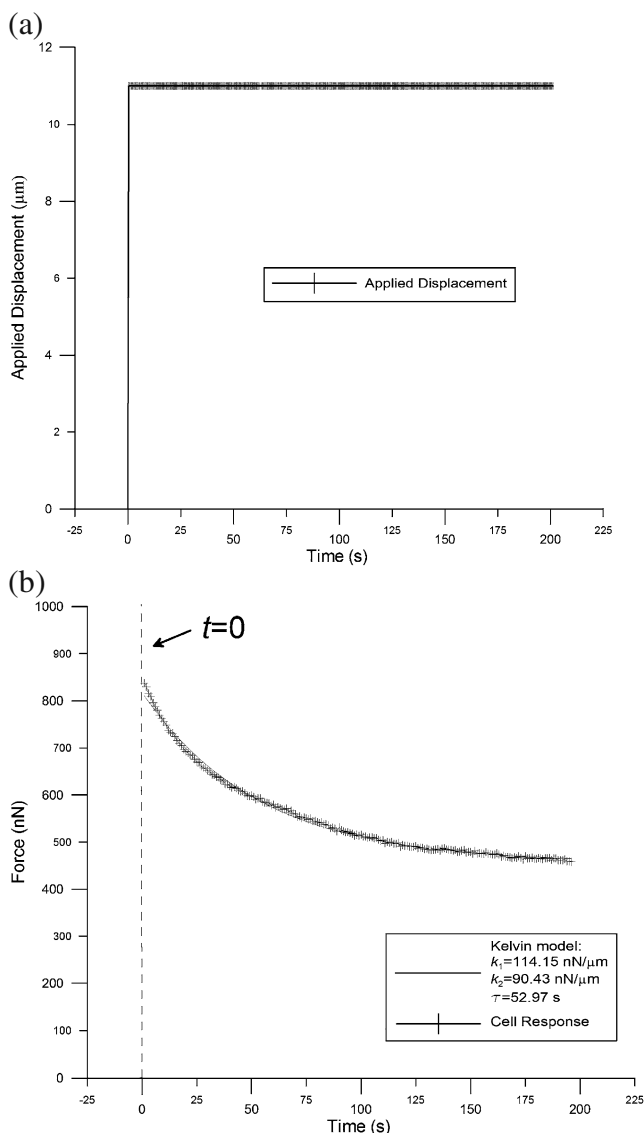

Fig. 5 A step input is applied to the cell platform (a). The viscoelastic response of the cell was modeled using the Kelvin model (b)
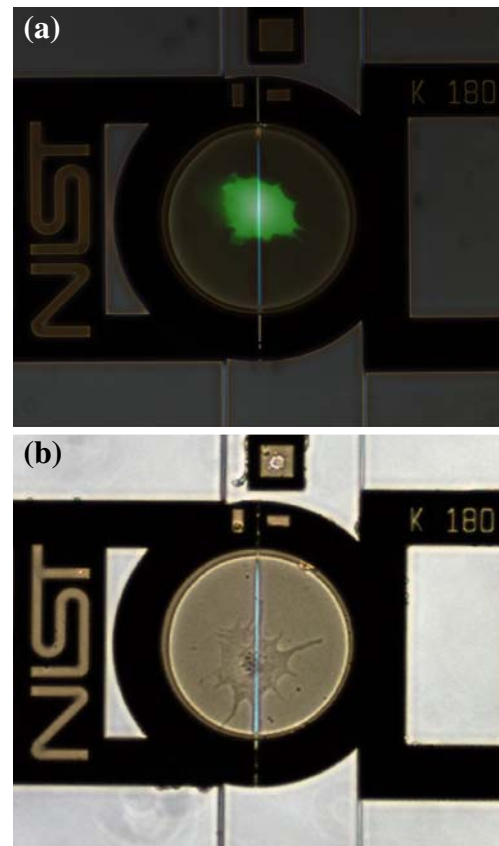

Fig. 6 A single fibroblast is imaged on the transparent cell platform via a live/dead fluorescence assay (a) and in phase contrast (b)

4 Conclusion

We have developed and tested a microfabricated device designed to allow quantitative force-displacement data while imaging a single, adherent cell in real-time. The device was fabricated by use of a single-layer SCS process utilizing commercially available SOI wafers. The device consists of a circular, transparent cell platform on which a single cell is placed. A displacement is applied to the cell and the force on the cell can be calculated.

The device was demonstrated on a single fibroblast cell. A step input was provided for the displacement and the viscoelastic response of the cell was observed. The standard linear model was used to model the response. A fibroblast cell was imaged while adhered to the cell platform in phase contrast and via fluorescence to demonstrate the transparent platform.

The imaging capabilities have the potential to allow observation of subcellular components in real-time while obtaining force-displacement measurements. Thus, correlations can be made between cytoplasmic constituents and the force response of the cell.

References

K.A. Addae-Mensah, J.P. Wikswo, Exp. Biol. Med. (2008). doi:10.3181/0710-MR-278

K.M. Ainslie, J.S. Garanich, R.O. Dull, J.M. Tarbell, J. Appl. Physiol. **98**, 242 (2005). doi:10.1152/japplphysiol.01006.2003

F.J. Alenghat, B. Fabry, K.Y. Tsai, W.H. Goldmann, D.E. Ingber, Biochem. Biophys. Res. Commun. **277**, 93 (2000). doi:10.1006/bbrc.2000.3636

A.R. Bausch, W. Möller, E. Sackmann, Biophys. J. **76**, 573 (1999)

J. Chen, B. Fabry, E.L. Schiffrin, N. Wang, Am. J. Physiol. Cell Physiol. **280**, C1475 (2001)

M.E. Chicurel, C.S. Chen, D.E. Ingber, Curr. Opin. Cell Biol. **10**, 232 (1998). doi:10.1016/S0955-0674(98)80145-2

L. Deng, X. Trepat, J.P. Butler, E. Millet, K.G. Morgan, D.A. Weitz et al., Nat. Mater. **5**, 636 (2006). doi:10.1038/nmat1685

J.P. Desai, A. Pillarisetti, A.D. Brooks, Annu. Rev. Biomed. Eng. **9**, 35 (2007). doi:10.1146/annurev.bioeng.9.060906.151940

N. Desprat, A. Richert, J. Simeon, A. Asnacios, Biophys. J. **88**, 2224 (2005). doi:10.1529/biophysj.104.050278

F. Di Palma, M. Douet, C. Boachon, A. Guignandon, S. Peyroche, B. Forest et al., Biomaterials **24**, 3139 (2003). doi:10.1016/S0142-9612(03)00152-2

E. Evans, A. Yeung, Biophys. J. **56**, 151 (1989)

E.A. Evans, R.M. Hochmuth, Biophys. J. **16**, 1 (1976)

B. Fabry, G.N. Maksym, J.P. Butler, M. Glogauer, D. Navajas, J.J. Fredberg, Phys. Rev. Lett. **87**, 148102 (2001). doi:10.1103/PhysRevLett.87.148102

B. Fabry, G.N. Maksym, J.P. Butler, M. Glogauer, D. Navajas, N.A. Taback et al., Phys. Rev. E Stat. Nonlin. Soft Matter Phys. **68**, 041914 (2003). doi:10.1103/PhysRevE.68.041914

E.L. Florin, V.T. Moy, H.E. Gaub, Science. **264**, 415 (1994). doi:10.1126/science.8153628

R.M. Hochmuth, Scand. J. Clin. Lab. Invest. Suppl. **156**, 63 (1981). doi:10.3109/00365518109097434

R.M. Hochmuth, R.E. Waugh, Annu. Rev. Physiol. **49**, 209 (1987). doi:10.1146/annurev.ph.49.030187.001233

K. Hyonchol, H. Arakawa, T. Osada, A. Ikai, Colloids. Surf. B. Biointerfaces. **25**, 33 (2002). doi:10.1016/S0927-7765(01)00299-5

A. Ignatius, H. Blessing, A. Liedert, D. Kaspar, L. Kreja, B. Friemert et al., Orthopade **33**, 1386 (2004). doi;10.1007/s00132-004-0735-z

P.A. Janmey, Physiol. Rev. **78**, 763 (1998)

P.A. Janmey, C.A. McCulloch, Annu. Rev. Biomed. Eng. **9**, 1 (2007). doi:10.1146/annurev.bioeng.9.060906.151927

T.J. Lardner, R.R. Archer, 262 (1994)

G. Lenormand, J.J. Fredburg, Biorheology **43**, 1 (2006)

C.M. Lo, M. Glogauer, M. Rossi, J. Ferrier, Eur. Biophys. J. **27**, 9 (1998). doi:10.1007/s002490050105

A. Maniotis, C. Chen, D. Ingber, Proc. Natl. Acad. Sci. USA. **94**, 849 (1997). doi:10.1073/pnas.94.3.849

A.B. Mathur, A.M. Collinsworth, W.M. Reichert, W.E. Kraus, G.A. Truskey, J. Biomech. **34**, 1545 (2001)

A. Minajeva, M. Kulke, J.M. Fernandez, W.A. Linke, Biophys. J. **80**, 1442 (2001)

M. Moretti, A. Prina-Mello, A.J. Reid, V. Barron, P.J. Prendergast, J. Mater. Sci. Mater. Med. **15**, 1159 (2004). doi:10.1023/B:JMSM.0000046400.18607.72

J.S. Park, J.S. Chu, C. Cheng, F. Chen, D. Chen, S. Li, Biotechnol. Bioeng. **88**, 359 (2004). doi:10.1002/bit.20250

G.K. Ragsdale, J. Phelps, K. Luby-Phelps, Biophys. J. **73**, 2798 (1997)

N.P. Rhodes, A.P. Shortland, A. Rattray, D.F. Williams, J. Mater. Sci. Mater. Med. **9**, 767 (1998). doi:10.1023/A:1008971406590

T. Saif, C.R. Sager, S. Coyer, Ann. Biomed. Eng. **31**, 950 (2003). DOI 10.1114/1.1591189

T. Saif, C. Sager, S. Coyer, American Society of Mechanical Engineers, Micro-Electromechanical Systems Division Publication (MEMS), 591 (2002)

N. Scuor, P. Gallina, H.V. Panchawagh, R.L. Mahajan, O. Sbaizero, V. Sergo, Biomed. Microdevices **8**, 239 (2006). doi:10.1007/s10544-006-8268-3

D. Serrell, T. Oreskovic, A. Slifka, R.L. Mahajan, D. Finch, Biomed. Microdevices. **9**, 267 (2007). doi:10.1007/s10544-006-9032-4

A. Soghomonians, A.I. Barakat, T.L. Thirkill, G.C. Douglas, Biol Reprod. (2005)

K. Svoboda, S.M. Block, Annu. Rev. Biophys. Biomol. Struct. **23**, 247 (1994)

O. Thoumine, A. Ott, J. Cell. Sci. **110**(Pt 17), 2109 (1997)

M. Tortonese, N. Maruyama, Micromachining and Imaging. **3009**, 53 (1997)

N. Wang, J.P. Butler, D.E. Ingber, Science. **260**, 1124 (1993)

S. Yamada, D. Wirtz, S.C. Kuo, Biophys. J. **78**, 1736 (2000)

A. Yamamoto, S. Mishima, N. Maruyama, M. Sumita, Biomaterials. **19**, 871 (1998)

S. Yang, T. Saif, Exp. Cell. Res. **305**, 42 (2005)

K.S. Zaner, P.A. Valberg, J. Cell. Biol. **109**, 2233 (1989)